Giant magnetoresistance of nickel-contacted carbon nanotubes

2007 J. Phys.: Condens. Matter 19 042201

(http://iopscience.iop.org/0953-8984/19/4/042201)

IOP FTC

INSTITUTE OF PHYSICS PUBLISHING JOURNAL OF PHYSICS: CONDENSED MATTER

J. Phys.: Condens. Matter **19** (2007) 042201 (7pp) doi:10.1088/0953-8984/19/4/042201

FAST TRACK COMMUNICATION

Giant magnetoresistance of nickel-contacted carbon nanotubes

Stavros Athanasopoulos[1,2], Steven W Bailey[1], Jaime Ferrer[3], Victor M García Suárez[1], Colin J Lambert[1], Alexandre R Rocha[4] and Stefano Sanvito[4]

[1] Department of Physics, Lancaster University, Lancaster LA1 4YB, UK
[2] Department of Physics, University of Bath, Bath, BA2 7AY, UK
[3] Departamento de Física, Universidad de Oviedo, 33007 Oviedo, Spain
[4] Department of Physics, Trinity College, Dublin 2, Republic of Ireland

E-mail: s.athanasopoulos@bath.ac.uk

Received 19 September 2006, in final form 13 November 2006
Published 12 January 2007
Online at stacks.iop.org/JPhysCM/19/042201

Abstract

We present *ab initio* theoretical results for the giant magnetoresistance of single-wall carbon nanotubes (CNT) in contact with nickel electrodes. These show that Ni atoms located on the surface or axis of CNT contacts can induce a significant magnetic moment on the carbon atoms. For non-gated, undoped CNTs, this produces room-temperature GMR ratios of between 45% and 100% of the anti-aligned conductance.

(Some figures in this article are in colour only in the electronic version)

Spin-polarized transport in carbon nanotubes (CNTs) connected to ferromagnetic contacts is receiving increasing interest, in part due to the promise of novel spintronic devices. Recent results suggesting that CNT-spintronic devices could soon become a reality include observations [1] of hysteretic magnetoresistance in Co-contacted nanotubes, which showed a resistance change of 9%, a measured magnetoresistance ratio of almost 100% in single-wall CNTs contacted to Fe electrodes [2, 3] and the possibility of contact-induced magnetism in CNTs [4–6]. Experiments also suggest ferromagnetic behaviour in rhombohedral C_{60} [7] and ferromagnetic and superconducting behaviour in highly orientated pyrolytic graphite [8].

In this letter, *ab initio* theoretical results are presented, which demonstrate how giant magnetoresistance (GMR) can arise in CNTs, contacted to nickel electrodes. We consider a clean section of single-wall CNT of length L, in contact with CNT regions containing Ni impurities along their axes or on their surfaces, as shown in figure 1. This situation may be deliberately engineered, or, for Ni electrodes in contact with a CNT, may occur, if Ni atoms migrate along either the axes or the surfaces of the CNT regions closest to the electrodes. Our central result, summarized in figure 2, is that Ni atoms located on the surface or axis of the

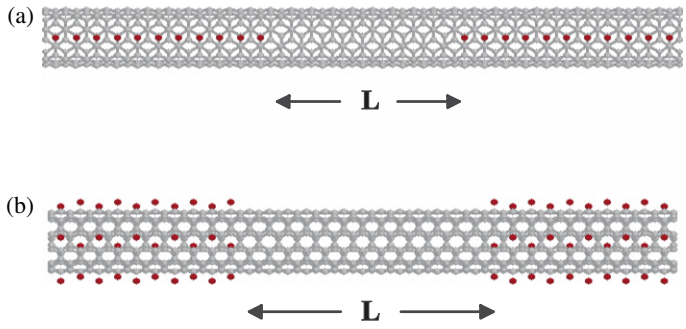

Figure 1. Armchair carbon nanotube in contact with ferromagnetic electrodes: (a) Ni atoms encapsulated along the axis of a CNT; (b) Ni atoms located on the surface of a CNT.

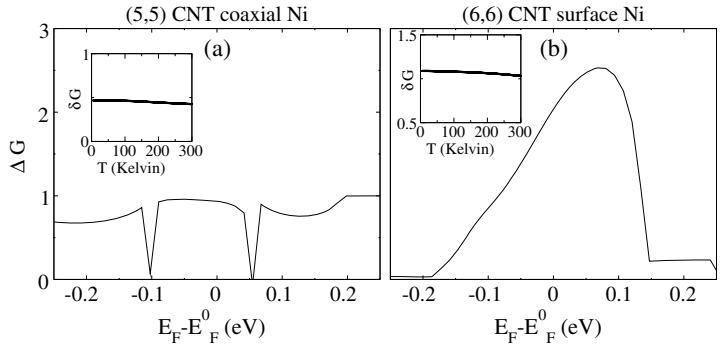

Figure 2. The zero-temperature magnetoconductance ΔG (in units of e^2/h) as a function of the Fermi energy E_F, for (a) a (5, 5)-Ni CNT in contact with a clean CNT of length $L = 4$ cells and (b) a (6, 6)-Ni coated CNT in contact with a clean CNT of length $L = 2$ cells. For E_F equal to the undoped Fermi energy E_F^0, the insets show the finite-temperature GMR ratio δG, obtained by integrating over Fermi distributions of incoming electrons from the left and right contacts.

CNT contacts can induce a significant magnetic moment on the carbon atoms, leading to room-temperature GMR ratios of between 45% and 100% of the anti-aligned conductance.

To obtain these results, the zero-bias conductance is computed via the Landauer formula $G = G_0 T(E_F)$, where $G_0 = e^2/h$, and $T(E_F)$ is the transmission coefficient, evaluated at the Fermi energy E_F. In the absence of spin-flip scattering, $T(E_F)$ is obtained by summing the transmission coefficients of two independent spin fluids, to yield $T(E_F) = T^{\uparrow}(E_F) + T^{\downarrow}(E_F)$. In figure 2 and in what follows, recognizing that the Fermi energy E_F can be varied by external doping and/or external gating, we present results for a range of energies in the vicinity of the Fermi energy E_F^0 of the un-doped, non-externally gated structure. When the magnetic moments of the electrodes are aligned in parallel (anti-parallel), we denote the dimensionless conductance G/G_0 by G_{++} (G_{+-}). The dimensionless magnetoconductance ΔG, plotted in figure 2, is then given by $\Delta G = G_{++} - G_{+-}$ and the GMR ratio is plotted in the insets by $\delta G = G/G_{+-}$.

We compute these transport coefficients using a Green function scattering technique, developed in reference [9], combined with a Hamiltonian generated using the first-principles density functional theory code, SIESTA [10]. Core electrons are replaced by non-local, norm-conserving pseudopotentials (Troulier–Martins) [13] and the wavefunctions of valence

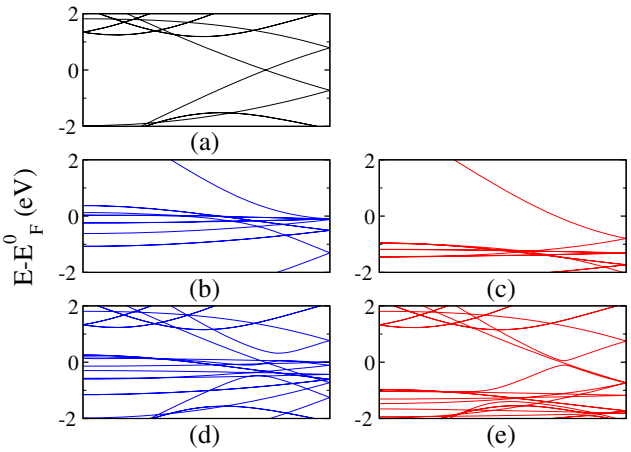

Figure 3. Band structure for (a) (5, 5) CNT, (b) majority and (c) minority spin carriers of a 1D Ni chain, (d) majority and (e) minority spin carriers for a (5, 5) CNT with coaxial Ni atoms.

electrons expanded over linear combinations of numerical orbitals. Multiple basis functions are used for each angular momentum (zetas) and in what follows double-zeta singly polarized are employed for carbon s and p orbitals and a double-zeta singly-polarized s and d orbitals for nickel. We also use the generalized gradient approximation (GGA) with the Perdew–Burke–Ernzerhof [12] parameterization of the exchange–correlation potential. Real-space integrations are performed on a regular grid with an equivalent plane-wave mesh cutoff of 400 Ryd. Atomic positions are relaxed until all force components are smaller than 0.02 eV Å^{-1}. After relaxation, the real-space Hamiltonian for the system is fed into our Green function technique [9][5] to yield the transmission coefficients of the device.

We first consider the case of an armchair CNT with Ni atoms located on the axis of the tube, shown in figure 1(a), and present results for a (5, 5) CNT, whose unit cell comprises 40 C and two Ni atoms and a lattice constant of 4.92 Å. (Two unit cells of the original CNT must be included explicitly, since overlap elements extend further than a single unit cell of the original CNT.) After relaxing all atomic positions, the Ni atoms are found to remain near their initial positions on the axis of the tube, and a total magnetization of $M = 2.54\ \mu_B$ per unit cell is obtained. Figures 3(d) and (e) shows the band structure for majority and minority spin carriers, respectively. For comparison, figure 3(a) shows the band structure of a clean (5, 5) CNT with a unit cell of 40 C atoms and figures 3(b) and (c) the majority and minority band structures of an isolated one-dimensional (1D) Ni chain. The Ni chain calculation of figures 3(b) and (c) shows that majority bands of low dispersion are present near E_F^0, whereas the minority-spin bands lie approximately -1 eV below E_F^0. Figures 3(d) and (e) suggest that this situation persists when the Ni chain is located along the axis of the CNT. To confirm this suggestion, we present in figure 4(a) the projected density of states (PDOS) for the 1D Ni chain, projected onto the 3d orbital, along with the total density of states. This shows that the main contribution to majority-spin states at the Fermi energy comes from the 3d states. Similarly the PDOS on the 3d Ni orbitals of a (5, 5) CNT with Ni along the axis is presented in figure 4(b), where we also show the density of states projected onto all 40 C atoms of the unit cell. (Note that, by symmetry, all Ni atoms possess the same PDOS.) Again, the 3d states dominate the majority-

[5] Recently, this has been developed into a new non-equilibrium Greens function code, SMEAGOL (Spin and Molecular Electronics in an Atomically-Generated Orbital Landscape. www.smeagol.tcd.ie) [11].

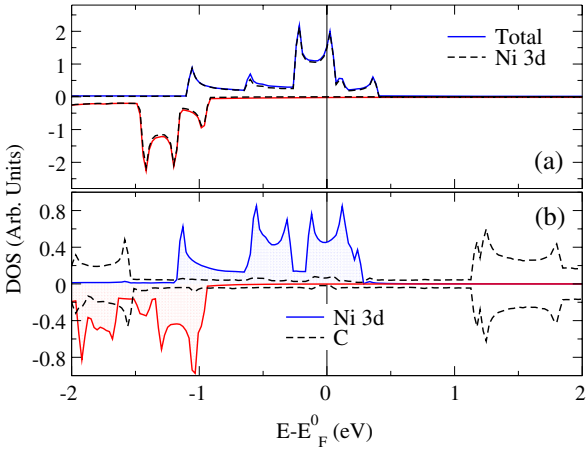

Figure 4. (a) Projected density of states for a Ni chain for the 3d orbitals and total DOS; (b) density of states for a (5, 5) CNT with coaxial Ni atoms projected onto the 3d orbitals of the Ni atoms and DOS projected to the carbon atoms.

spin PDOS at E_F^0, but make a negligible contribution to the minority-spin carriers at E_F^0. As shown below, these pinned 3d Ni states play a key role in determining the magnitude GMR in such structures.

As a prelude to a full transport calculation, we first obtain an upper bound for the conductances in the aligned and anti-aligned configurations, by counting the number of open channels in the band structures of figure 3 [6]. For electrodes with parallel alignment, we approximate the structure of figure 1(a) by an infinite CNT with Ni atoms along the axis and all moments aligned. The dimensionless conductances $G^{\sigma}_{++}(E_F) = T^{\sigma}(E_F)$ and $G_{++}(E_F) = G^{\uparrow}_{++}(E_F) + G^{\downarrow}_{++}(E_F)$ are then given by $G^{\uparrow}_{++}(E_F) = N^{\uparrow}(E_F)$ and $G^{\downarrow}_{++}(E_F) = N^{\downarrow}(E_F)$, where $N^{\sigma}(E_F)$ is the number of open scattering channels for electrons of spin σ. The integers $N^{\sigma}(E_F)$ are readily obtained from figure 3(a) by noting how many bands cross a horizontal line of constant energy $E = E_F$. For a clean CNT connected to ferromagnetic electrodes with anti-aligned moments, we approximate the structure of figure 1(a) by an infinite CNT with Ni atoms along the axis, but with the Ni moments of one half of the chain anti-aligned relative to those of the other half. In this case, the conductance is $G_{+-}(E_F) = 2G^{\uparrow}_{+-}(E_F) = 2G^{\downarrow}_{+-}(E_F)$, where $G^{\sigma}_{+-}(E_F) = T^{\sigma}(E_F)$. Recognizing that transmitted spins must have open channels in both halves of the chain leads us to approximate $G_{+-}(E_F)$ by $G_{+-}(E_F) = 2\ \min\{N^{\uparrow}(E_F), N^{\downarrow}(E_F)\}$. The above argument ignores electron scattering and yields upper bounds for $G_{++}(E_F)$ and $G_{+-}(E_F)$.

Since $N^{\sigma}(E_F)$ is determined from the band structures of the Ni–CNT composites, shown in figure 3, the above estimates are much easier to obtain than the results of a more computationally expensive scattering calculation. However, it should be noted that, whereas this 'zero-scattering' picture yields upper bounds for G_{++} and G_{+-}, there is no such upper bound on their difference and therefore the resulting estimate for ΔG should be treated with more caution. For Ni along the axis, using the band structure of figure 3, the resulting values for the dimensionless conductances G_{++} and G_{+-} are presented in figures 5(a), which combine to yield the 'zero-scattering' prediction for ΔG shown in figure 5(b). For Ni along the axis, at $E_F = E_F^0$ the 'zero-scattering' conductance for parallel (anti-parallel) alignment is $G_{++}(E_F^0) = 8$ ($G_{+-}(E_F^0) = 2$), which yields a 'zero-scattering' prediction of $\Delta G = 6$.

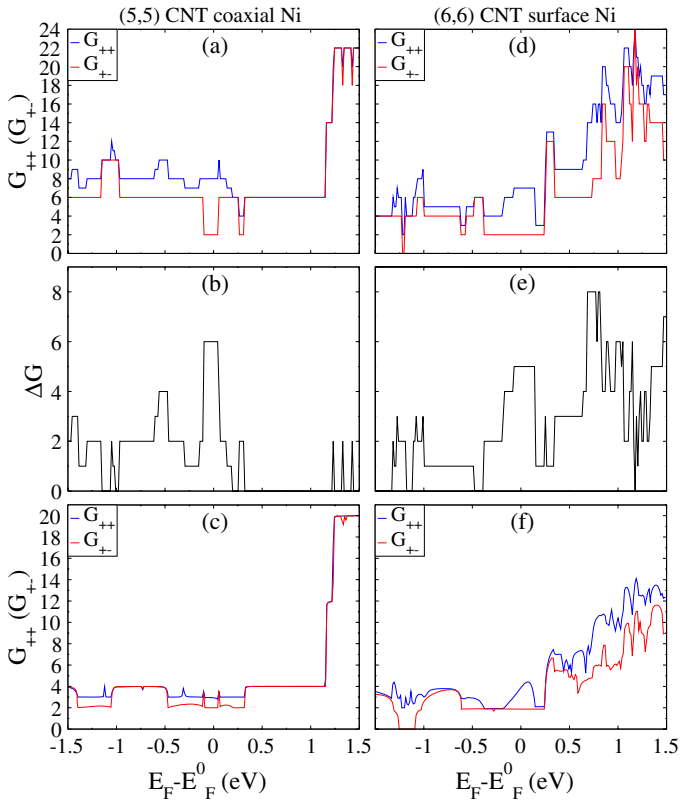

Figure 5. (a) and (b) Step edge model of GMR for the (5, 5)-Ni CNT; (c) differential conductance for the ferromagnetic and antiferromagnetic alignment and for a (5, 5)-Ni CNT in contact with a clean CNT of length $L = 4$ cells. (d) and (e) Step edge model of GMR for Ni on the surface of a (6,6) CNT; (f) differential conductance for the ferromagnetic and antiferromagnetic alignment for a (6,6)-Ni coated CNT in contact with a clean CNT of length $L = 2$ cells.

To obtain the full *ab initio* result, we now consider two semi-infinite (5, 5) CNT-Ni leads, in contact with a clean CNT of length L unit cells. For $L = 4$, our results for G_{++} and G_{+-} are shown in figure 5(c), while the corresponding ΔG is plotted in figure 2(a). The corresponding magnetoconductance is $\Delta G \approx 1$ at $E = E_F$, yielding a GMR ratio $\delta G = \Delta G/G_{+-} \approx 52\%$, which is almost energy independent over a range of order 0.1 eV. As a consequence, as shown in the inset of figure 2(a), the corresponding thermally averaged magnetoconductance and GMR ratio are almost temperature independent.

Comparing figure 5(c) with (a) confirms that the zero-scattering model provides upper bounds for the conductances G_{++} and G_{+-} and, in addition, yields the correct qualitative energy dependence on the scale of electron volts. In the full *ab initio* calculation, conductances are suppressed, because the absence of Ni in the region of length L removes a significant number of conducting channels. Furthermore, this suppression is spin dependent and therefore the zero-scattering values of ΔG are a significant overestimate of the *ab initio* value. Figure 5(c) also shows that, at certain energies, small negative values of ΔG occur. These multiple-scattering effects are sensitive to the length L of the Ni-free region [14, 15] and, unlike the main band-structure-driven magnetoconductance described above, are smeared out by thermal and ensemble averaging.

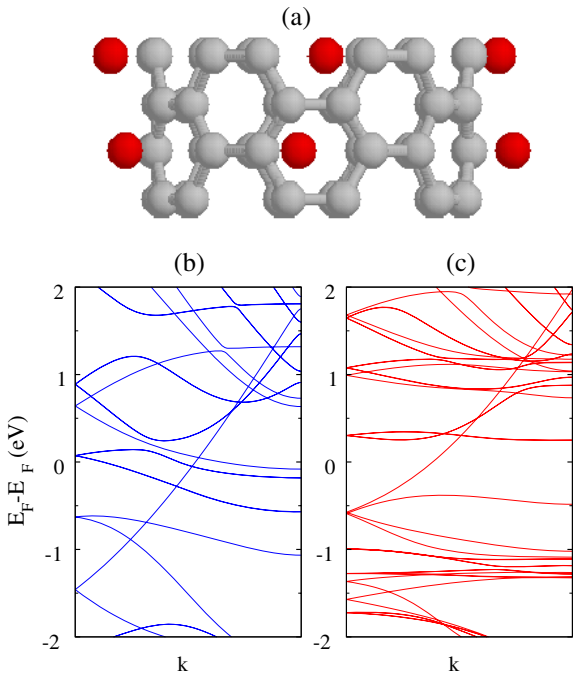

Figure 6. (a) The unit cell of a (6,6) CNT with Ni atoms on the surface. Band structure of the system for (b) majority and (c) minority spin carriers.

As a second source of magnetoconductance, we now consider the structure shown in figure 1(b), where Ni atoms are located on the surface of a CNT. It is known that Ni adsorbed on a graphene sheet loses its magnetic moment [16]. As a check on our codes, we have performed separate calculations confirming this feature and find that the Ni atoms relax above the centre of the graphene hexagons with a C–Ni bond of length ≈2.19 Å. In contrast, we find that Ni atoms near the surface of a CNT retain a finite moment and furthermore induce a significant moment on the carbon atoms. To demonstrate this, we show *ab initio* results for an infinite (6,6) CNT. The unit cell now is a ring of 48 C atoms, with six Ni atoms near the surface of the tube and a lattice constant of 4.92 Å. This doubling of the unit cell is necessary, since Ni atoms are placed above the centres of hexagons with one Ni atom per two carbon rings on the circumference, while, in the direction of the tube axis, Ni atoms are placed adjacent to the non-occupied rings of the previous CNT unit cell, as shown in figure 6(a). For this calculation, we have used a mesh cutoff of 600 Ryd and a double-zeta polarized basis set for nickel and carbon. After full relaxation of the atomic coordinates, the Ni atoms remain above the centre of the hexagons with an average C–Ni distance ≈2.21 Å. The magnetic moment for Ni is found to be $M = 1.66\ \mu_B$ per Ni atom and the total moment for the C atoms $M = -0.52\ \mu_B$, resulting in an induced total moment of $M = 9.42\ \mu_B$ for the whole unit cell. There is also a considerable charge transfer of $0.73(-e)$ from nickel atoms to carbon. The band structure for majority spin carriers and for minority spin carriers is shown in figures 6(b) and (c), respectively, and the resulting 'zero-scattering' results are shown in figures 5(d) and (e). Figure 5(f) shows the full *ab initio* transport calculation for two semi-infinite (6,6)-CNT-Ni leads in contact with a clean tube of length $L = 2$ cells. Results for G_{++} and G_{+-} are shown in figure 5(f), while figure 2(b) shows the magnetoconductance ΔG. For $E_F = E_F^0$, these results yield $\Delta G \approx 2$ and a GMR ratio δG

of order 100%. For the case of Ni on the CNT surface, the zero-scattering prediction presented in figure 5(d) again reflects the qualitative features of the exact results shown in figure 5(f), but the zero-scattering values of ΔG are significantly over-estimated.

In conclusion, we have performed *ab initio* calculations of GMR in Ni-doped armchair CNTs and predict values for the GMR ratio δG of up to 100%, which are almost temperature independent. The magnetoconductance ΔG for a CNT with Ni on the surface is more than two times larger than the ΔG of a CNT with coaxial Ni. A knowledge of the band structure alone is found to be a guide to qualitative features of the spin conductances, but reliable results for the magnetoconductance require a full *ab initio* treatment.

This work is supported in part by the European Union's FP6 programme under contract no. MRTN-CT-2003-504574, the UK Engineering and Physical Sciences Research Council (EPSRC) and a Royal Society joint project with Ireland. ARR and SS thank the Science Foundation of Ireland for financial support. JF and VMG-S also acknowledge support from the Spanish Ministerio de Ciencia y Tecnología and Ministerio de Educación, Cultura y Deportes project no. BFM2003-03156.

References

[1] Tsukagoshi K, Alphenaar B W and Ago H 1999 *Nature* **401** 572
[2] Jensen A, Nygard J and Borggreen J 2003 *MSS2002 Proc.* ed H Takayanagi and J Nitta (Singapore: World Scientific) pp 33–7
[3] Lindelof P E, Borggreen J, Jensen A, Nygard J and Poulsen P R 2002 *Nobel Symp. Proc. 2001*; *Phys. Scr.* T **102** 22
[4] Céspedes O, Ferreira M S, Sanvito S, Kociak M and Coey J M D 2004 *J. Phys.: Condens. Matter* **16** L155
[5] Ferreira M S and Sanvito S 2003 *Phys. Rev.* B **68** 054425
[6] Lambert C J, Athanasopoulos S, Grace I M and Bailey S W 2004 Computer modelling and simulation of materials, Part C: modeling and simulating materials nanoworld *Proc. 3rd Int. CIMTEC Conf.* p 355
[7] Makarova T L, Sundqvist B, Höhne R, Esquinazi P, Kopelevich Y, Scharff P, Davydov V A, Kashevarova L S and Rakhmanina A V 2001 *Nature* **413** 716
[8] Kopelevich Y, Esquinazi P, Torres J H S and Moehlecke S 2000 *J. Low Temp. Phys.* **119** 691
[9] Sanvito S, Lambert C J, Jefferson J H and Bratkovsky A 1999 *Phys. Rev.* B **59** 11936
[10] Soler J M, Artacho E, Gale J D, Garcia A, Junquera J, Ordejón P and Sánchez-Portal D 2002 *J. Phys.: Condens. Matter* **14** 2745–79
[11] Reily Rocha A, García-Suárez V M, Bailey S W, Lambert C J, Ferrer J and Sanvito S 2005 *Nat. Mater.* **4** 355
[12] Perdew J P, Burke K and Ernzerhof M 1996 *Phys. Rev. Lett.* **77** 3865
[13] Troullier N and Martins J L 1991 *Phys. Rev.* B **43** 1993
[14] Iwo Babiaczyk W and Bulka B R 2002 *Preprint* cond-mat/0207672
[15] Liang W, Bockrath M, Bozovic D, Hafner J H, Tinkham M and Park H 2001 *Nature* **411** 665
[16] Duffy D M and Blackman J A 1998 *Phys. Rev.* B **58** 7443